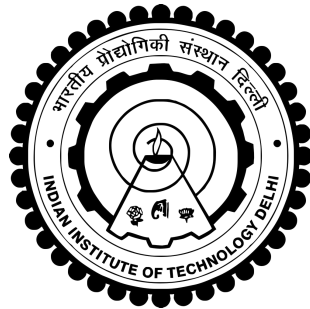


**Coupled Electrothermal Modelling with Phase Change Material  
(PCM) and Hybrid Thermal Management for Li-ion Batteries**

**SAGAR VASHISHT**



**DEPARTMENT OF ENERGY SCIENCE AND ENGINEERING**

**INDIAN INSTITUTE OF TECHNOLOGY DELHI**

**July 2025**

© Indian Institute of Technology Delhi (IITD), New Delhi, 2025

**Coupled Electrothermal Modelling with Phase Change Material  
(PCM) and Hybrid Thermal Management for Li-ion Batteries**

*by*

**Sagar Vashisht**

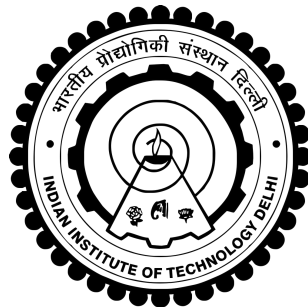
**Department of Energy Science and Engineering**

*Submitted*

*In fulfillment of the requirements of the degree of*

**Doctor of Philosophy**

*to the*



**INDIAN INSTITUTE OF TECHNOLOGY DELHI**

**HAUZ KHAS, NEW DELHI-110016 INDIA**

**July 2025**

*Dedicated to my family members*

## **DECLARATION**

I declare that this written submission represents my ideas in my own words. I have adequately cited and referenced the original sources when including others' ideas and words. I further declare that I have adhered to all academic honesty and integrity principles and have not misrepresented, fabricated, or falsified any idea, data, fact, or source in my submission.

This thesis is composed of my original work and contains no material previously published or written by another person, except where due reference has been made in the text. I have clearly stated the contributions of others to jointly authored works included in this thesis.

I acknowledge that an electronic copy of my thesis must be lodged with the university library, subject to the policy and procedures of the Indian Institute of Technology Delhi.

Sagar Vashisht

## CERTIFICATE

This is to certify that the thesis titled **Coupled Electrothermal Modelling with Phase Change Material (PCM) and Hybrid Thermal Management for Li-ion Batteries**, submitted by **Mr. Sagar Vashisht**, to the Indian Institute of Technology, Delhi, for the award of the degree of **Doctor of Philosophy**, is a Bonafide record of the original research work done by him under my supervision and guidance at Department of Energy Science and Engineering, Indian Institute of Technology Delhi. The contents of this thesis, in full or in parts, have not been submitted to any other Institute or University for the award of any degree or diploma.

*Dibakar Rakshit*

(Dr. Dibakar Rakshit)  
Professor,  
Department of Energy Science and Engineering  
Indian Institute of Technology Delhi  
Hauz Khas, New Delhi - 110016  
India



## ACKNOWLEDGEMENTS

This thesis has been a journey of exploration, growth, and perseverance, made possible by the unwavering support, guidance, and encouragement of many individuals to whom I owe my deepest gratitude.

First and foremost, I would like to express my heartfelt thanks to my supervisor, Prof. Dibakar Rakshit, for his invaluable guidance, patience, and encouragement throughout my research. His insights and mentorship have been instrumental in shaping my work and pushing me to achieve the best version of myself as a researcher.

I extend my utmost gratitude and sincerely thank Dr. Satyam Panchal, Prof. Michael Fowler, and Prof. Roydon Fraser from the University of Waterloo, Canada. Their generous support in providing experimental data for my initial work, valuable suggestions, and constructive feedback greatly enriched the quality of my research. I am genuinely grateful for their involvement in my academic journey.

I would also like to convey my sincere thanks to my research committee members, including Prof. Anil Verma (Department of Chemical Engineering, IIT Delhi), Prof. Vamsi Krishna Komarala, and Prof. Kaushik Saha (Department of Energy Science and Engineering, IIT Delhi)—for their insightful comments and valuable suggestions during the various stages of my research evaluation. Their input has been crucial in refining and steering my work in the right direction.

My heartfelt gratitude goes to my senior and fellow lab members: Dr. Ashish Kumar, Dr. Alok Kumar Ray, Dr. Pranaynil Saikia, Dr. S Sai Saran Yagnamurthy, Dr. Sana Fatima Ali, Dr. Ashima Verma, Dr. Tewodros Ashagre Belay, Dr. Abhishek Agrawal, Mr. Rahul Kumar Sharma,

Mr. Mohit Barthwal, Mr. Rahul Verma, Mr. Mohit Murarka, Mr. Suyash Vikram, Mr. Jibin M Joy, Mr. Faraz P Junnaid, Mr. Sumit Singh, Mr. Dilshad Ahmad, Mr. Aakash Sadar, Mr. Ikhtedar Husain Rizvi, Mr. Mallayya and all my lab mates. Your support, camaraderie, and encouragement kept my spirits high during the challenging phases of my research work. I am equally grateful to my friends, both within and outside the campus, for being my pillars of strength and making this journey less daunting. I am also profoundly thankful to the IIT Delhi staff and the Department of Energy Science and Engineering for their constant support and assistance whenever needed.

To my family, my deepest gratitude goes to my mother, who taught me to find joy and meaning in life's little moments, and to my father, who exemplified dedication, selflessness, and unwavering support.

This thesis is not just the culmination of my efforts but a reflection of the collective support, kindness, and encouragement I have received from everyone along the way. For that, I am genuinely grateful.

Sagar Vashisht

## ABSTRACT

The growing integration of renewable energy sources and the electrification of transport systems have increased the demand for efficient and reliable energy storage technologies. Lithium-ion batteries (Li-ion) are at the forefront of this transition due to their high energy density, long cycle life, and efficiency. However, their performance and safety are susceptible to temperature fluctuations. In electric vehicles (EVs), elevated or non-uniform temperatures can cause degradation, efficiency loss, and thermal runaway, posing safety risks.

This thesis presents a multi-level framework combining experimental characterization, electrothermal modelling, deep learning-based prediction, and advanced thermal management strategies. Temperature- and state of charge (SoC) dependent parameters such as open-circuit voltage, internal resistance, and entropic heat were extracted through experiments. These parameters inform the development of electrothermal models for two chemistries: LFP (prismatic) and NMC (cylindrical). The modelling includes resistance-based approaches and equivalent circuit models with inductive elements, enabling accurate prediction of temperature and voltage behaviour across varied discharge conditions. To enhance prediction under variable operating environments, data-driven models including Long Short-Term Memory (LSTM), Gated Recurrent Unit (GRU), and Transformer were trained on datasets collected at 4 °C, 24 °C, and 43 °C. These models estimate SoC, voltage, and temperature while capturing electrothermal dynamics and ageing indicators such as capacity fade and resistance growth. This integration of machine learning supports real-time monitoring and decision-making for battery management systems.

Thermal management solutions are then explored through a detailed numerical investigation of passive cooling with Phase Change Materials (PCMs). The effect of discharge

rate, melt fraction, and PCM layer thickness (1.25 mm, 2.50 mm, and 5.00 mm) is analyzed to identify optimal configurations that maintain thermal safety without overdesign. Performance metrics such as the Cell Cooling Coefficient and PCM Cooling Enhancement Factor are introduced. Building on this, an AHP-TOPSIS framework is applied to rank over 110 commercially available PCMs based on ten thermophysical and safety attributes. The simulation results guide the selection to ensure compatibility between PCM thermal properties, discharge-dependent heat loads, and optimal thickness configuration. The study also compares PCM-based cooling with passive immersion techniques using dielectric liquids like water-glycol, silicone, and mineral oil. A hybrid battery thermal management system is developed by integrating PCM with a liquid cooling jacket to improve thermal regulation beyond passive methods. A vehicle-level hybrid framework is also constructed in MATLAB Simulink to simulate coupling between an electric vehicle's battery and cabin thermal systems, allowing analysis of shared thermal loads and energy consumption.

Overall, this research delivers a scalable and technically rigorous strategy for improving the safety, thermal stability, and performance of Li-ion batteries. The work offers actionable insights for real-time diagnostics and future battery system development by integrating electrothermal modelling, machine learning, and advanced cooling design. It also contributes to sustainability by supporting clean energy technologies aligned with the UN Sustainable Development Goals (SDG 7 and SDG 13) and India's FAME and National Electric Mobility Mission.

Keywords: Electrothermal modelling; Lithium-ion battery; Phase Change Materials; Deep learning; Hybrid thermal management systems

## सारांश

अक्षय ऊर्जा स्रोतों के बढ़ते एकीकरण और परिवहन प्रणालियों के विद्युतीकरण ने कुशल और विश्वसनीय ऊर्जा भंडारण प्रौद्योगिकियों की मांग को बढ़ा दिया है। लिथियम-आयन बैटरी (ली-आयन) अपने उच्च ऊर्जा घनत्व, लंबे चक्र जीवन और दक्षता के कारण इस परिवर्तन में सबसे आगे हैं। हालांकि, उनका प्रदर्शन और सुरक्षा तापमान के उतार-चढ़ाव के प्रति संवेदनशील हैं। इलेक्ट्रिक वाहनों (ईवी) में, ऊंचा या असमान समान तापमान क्षरण, दक्षता में कमी और थर्मल रनवे का कारण बन सकता है, जिससे सुरक्षा जोखिम पैदा हो सकता है।

यह शोध-प्रबंध प्रायोगिक लक्षण-वर्णन, विद्युत-तापीय मॉडलिंग, गहन अधिगम-आधारित पूर्वानुमान और उन्नत तापीय प्रबंधन रणनीतियों को मिलाकर एक बहु-स्तरीय रूपरेखा प्रस्तुत करता है। तापमान और आवेश की अवस्था (SoC) पर निर्भर प्राचल, जैसे कि खुला-परिपथ वोल्टेज, आंतरिक प्रतिरोध और एन्ट्रॉपी ऊष्मा, प्रयोगों के माध्यम से निकाले गए। ये प्राचल दो रसायन विज्ञानों: LFP (प्रिज़मैटिक) और NMC (सिलेंडरनुमा) के लिए विद्युत-तापीय मॉडल के विकास को सूचित करते हैं। इस मॉडलिंग में प्रतिरोध-आधारित दृष्टिकोण और प्रेरक तत्वों वाले समतुल्य परिपथ मॉडल शामिल हैं, जो विभिन्न निर्वहन स्थितियों में तापमान और वोल्टेज व्यवहार का सटीक पूर्वानुमान लगाने में सक्षम बनाते हैं। परिवर्तनशील परिचालन परिवेशों में पूर्वानुमान को बेहतर बनाने के लिए, दीर्घ-अल्पकालिक स्मृति (LSTM), गेटेड आवर्तक इकाई (GRU), और ट्रांसफार्मर सहित डेटा-संचालित मॉडलों को 4°C, 24°C और 43°C पर एकत्रित डेटासेट पर प्रशिक्षित किया गया। ये मॉडल विद्युत-तापीय गतिकी और क्षमता क्षीणन तथा प्रतिरोध वृद्धि जैसे आयु सूचकों को ग्रहण करते हुए SoC, वोल्टेज और तापमान का अनुमान लगाते हैं। मशीन अधिगम का यह एकीकरण बैटरी प्रबंधन प्रणालियों के लिए वास्तविक समय की निगरानी और निर्णय लेने में सहायक होता है।

तत्पश्चात, ताप प्रबंधन समाधानों का अन्वेषण चरणबद्ध रूप से फेज़ चेंज मटेरियल (पीसीएम) आधारित पैसिव कूलिंग के संख्यात्मक विश्लेषण के माध्यम से किया गया है। डिस्चार्ज दर, मेल्ट फ्रैक्शन, और पीसीएम

परत की मोटाई (1.25 मिमी, 2.50 मिमी, और 5.00 मिमी) के प्रभाव का विश्लेषण किया गया है ताकि ऐसे विन्यास की पहचान की जा सके जो अधिक डिज़ाइन किए बिना तापीय सुरक्षा बनाए रखें। प्रदर्शन संकेतकों जैसे सेल कूलिंग गुणांक (Cell Cooling Coefficient) और पीसीएम कूलिंग संवर्धन गुणांक (PCM Cooling Enhancement Factor) को परिभाषित किया गया है। इसके आधार पर, एक AHP-TOPSIS रूपरेखा को लागू किया गया है, जिसमें दस थर्मोफिज़िकल और सुरक्षा गुणों के आधार पर 110 से अधिक वाणिज्यिक पीसीएम को रैंक किया गया है। सिमुलेशन परिणाम पीसीएम की तापीय विशेषताओं, डिस्चार्ज-निर्भर ऊष्मा भार, और इष्टतम मोटाई कॉन्फ़िगरेशन के बीच अनुकूलता सुनिश्चित करने में मार्गदर्शन करते हैं। अध्ययन में पीसीएम-आधारित कूलिंग की तुलना पैसिव इमर्शन तकनीकों से भी की गई है, जिसमें जल-ग्लाइकोल, सिलिकॉन, और मिनरल ऑयल जैसे डाइइलेक्ट्रिक द्रवों का उपयोग किया गया है। इसके अतिरिक्त, एक हाइब्रिड बैटरी थर्मल प्रबंधन प्रणाली विकसित की गई है जिसमें पीसीएम को तरल शीतलन जैकेट के साथ एकीकृत किया गया है, ताकि पैसिव तरीकों की तुलना में उन्नत तापीय नियंत्रण प्राप्त किया जा सके। MATLAB सिमुलिक में एक वाहन-स्तरीय हाइब्रिड ढांचा भी निर्मित किया गया है, जो इलेक्ट्रिक वाहन की बैटरी और केबिन थर्मल प्रणालियों के बीच युग्मन का अनुकरण करता है, जिससे साझा ऊष्मा भार और ऊर्जा खपत का विश्लेषण संभव होता है।

समग्र रूप से,, यह शोध लिथियम-आयन बैटरियों की सुरक्षा, तापीय स्थिरता और प्रदर्शन में सुधार के लिए एक मापनीय और तकनीकी रूप से सुदृढ़ रणनीति प्रदान करता है। यह कार्य इलेक्ट्रोथर्मल मॉडलिंग, मशीन लर्निंग और उन्नत शीतलन डिज़ाइन को एकीकृत करके वास्तविक समय निदान और भविष्य की बैटरी प्रणाली के विकास के लिए व्यावहारिक अंतर्दृष्टि प्रदान करता है। यह संयुक्त राष्ट्र सतत विकास लक्ष्यों (एसडीजी 7 और एसडीजी 13) और भारत के FAME और राष्ट्रीय इलेक्ट्रिक मोबिलिटी मिशन के अनुरूप स्वच्छ ऊर्जा प्रौद्योगिकियों का समर्थन करके स्थिरता में भी योगदान देता है।

मुख्य शब्द (कीवर्ड): इलेक्ट्रोथर्मल मॉडलिंग; लिथियम-आयन बैटरी; फेज़ चेंज मटेरियल; डीप लर्निंग; हाइब्रिड थर्मल प्रबंधन प्रणालियां

# Contents

	Page No.
CERTIFICATE	i
ACKNOWLEDGEMENTS	iii
ABSTRACT	v
List of Figures	xiii
List of Tables	xix
List of Symbols	xxi
1 Introduction	1
1.1 Background	1
1.2 Motivation	3
1.3 Overview of Lithium-ion Cell Design and Thermal Dynamics	5
1.4 Working Principles of Lithium-ion Cells	10
1.5 Heat Generation and Thermal Dynamics	11
1.6 Thermal Issues of Lithium-ion Batteries	15
1.7 Organization of Thesis	21
2 Literature Review	25
2.1 Preface	25
2.2 Battery Modelling Approaches	25
2.3 Battery Thermal Management System	33
2.4 Summary and conclusions of Literature Review	48
2.5 Problem Definition and Research Gaps	50
2.6 Objectives	51
3 Parametrization of Li-ion Battery Model	53
3.1 Preface	53
3.2 Parameterization Methods	54
3.3 Experimental Setup and Parameter Identification for LFP Li-ion Battery	61
3.4 Experimental Setup and Parameter Identification for NMC Li-ion Battery	66
3.5 Summary and conclusions	75
3.6 Closure	76
4 Electrothermal Model of LFP Li-ion Battery	77
4.1 Introduction	77
4.2 Numerical formulation and Problem definition	77
4.3 Governing equations for Electrothermal model	79
4.4 Electrothermal Model Definitions Based on Parameter Dependency	89
4.5 Results and discussion	91
4.6 Summary and conclusions	102
4.7 Closure	104
5 Electrothermal Model of NMC Li-ion Battery	105
5.1 Preface	105

5.2	Numerical Formulation and Problem Definition	106
5.3	Governing equations for Electrothermal model	109
5.4	Results and Discussion	121
5.5	Summary and conclusions	128
5.6	Closure	130
6	ML-Based Electrothermal Modelling and SoH Analysis	131
6.1	Preface	131
6.2	Methodology and Model Parameter	132
6.3	Source Data	133
6.4	Data processing	133
6.5	Model Architecture	135
6.6	Input Features and Feature Selection	144
6.7	Results and Discussion	148
6.8	Conclusion	163
6.9	Closure	164
7	PCM-Based Cooling System Modelling	167
7.1	Preface	167
7.2	Problem definition	168
7.3	Governing equations	171
7.4	Numerical method and grid study	177
7.5	Validation	179
7.6	Results and discussion	180
7.7	Conclusions	192
7.8	Closure	193
8	Multi-Criteria PCM Selection and Comparative Analysis of Passive Cooling Techniques	195
8.1	Preface	195
8.2	Hybrid AHP–TOPSIS Based PCM Selection Methodology	196
8.3	Analysis of the Proposed Methodology for PCM Selection	203
8.4	Thermal Behaviour Analysis and Correlation with TOPSIS Rankings	208
8.5	Comparative Evaluation of PCM and Passive Liquid Immersion Cooling	212
8.6	Comparative Analysis of Passive Cooling	217
8.7	Battery Pack-Level Performance	221
8.8	Conclusion	223
8.9	Closure	224
9	Hybrid Thermal Management System for Battery and Cabin Cooling	225
9.1	Preface	225
9.2	Numerical Evaluation of Hybrid Battery Thermal Management	225
9.3	Thermal Performance Evaluation of Hybrid Cooling	231
9.4	Simulink-Based Analysis of Integrated Battery and Cabin Cooling	232
9.5	Performance Evaluation of Battery and Cabin Cooling	236
9.6	Summary and Conclusions	238
9.7	Closure	239
10	Conclusions	241
10.1	Preface	241
10.2	Major outcomes	242
10.3	Scope for future work	244
11	References	245

A	Appendix A: Supplementary Tables	271
A.1	Experimental OCV and Internal Resistance Data	271
A.2	Experimental Uncertainty analysis	272
B	Appendix B: NMC 18650 Cell – EIS Spectra and Fitted Parameter Expressions	275
B.1	Electrochemical Impedance Spectra of NMC 18650 Cell	275
B.2	Polynomial Expressions for Electrothermal Parameters	275
C	Appendix C: Specifications and Experimental Data of INR 18650 Cell	279
C.1	Technical Specifications and Measured Data	279
D	Appendix D: Comparative Summary of Electrothermal Behaviour of LFP and NMC cells	281
D.1	Qualitative Comparison of Cell-Level Performance Parameters under Similar Discharge Conditions	281
	Brief Biodata and Publications	283



## List of Figures

Figure Number	Description	Page No.
Figure 1.1	(a) Global CO <sub>2</sub> emissions by sector with Breakdown of CO <sub>2</sub> emissions in the transportation sector worldwide 2022 [1] (b) Global CO <sub>2</sub> emissions by sector, 2019-2022 [2]	2
Figure 1.2	Annual number of fire incidents involving light-duty electric vehicles (EVs) and corresponding global EV market share from 2010 to 2023 [3,4]	4
Figure 1.3	Radar plots comparing different lithium-ion cathode chemistries (LCO, LMO, NMC, LFP, NCA, and LTO) [5]	9
Figure 1.4	Schematic representation of a lithium-ion cell showing physical structure, layered architecture, and charge-discharge pathways	11
Figure 1.5	Types of the heat generation within Li-ion Batteries (LiBs)	12
Figure 1.6	Relative capacity of LiFePO <sub>4</sub> w.r.t temperature [6]	16
Figure 1.7	(a) Discharge capacity (Ah) vs. cycle number at 85 °C and 120 °C [7] and (b) The impact of temperature and cycling on the capacity degradation [8]	19
Figure 1.8	Influence of temperature on Li-ion battery dynamics.	21
Figure 2.1	Categorization of battery models into white-box, grey-box, and black-box approaches.	26
Figure 2.2	Potential performance parameters for Battery thermal management system	34
Figure 2.3	(a) Classification of Battery Thermal Management Systems (BTMS) and (b) Key attributes, functions, and parameters influencing BTMS	36
Figure 2.4	Basic Schematic of Air based BTMS	37
Figure 2.5	A basic Schematic showing (a) Direct contact immersion, (b) Indirect contact thermal management techniques	38
Figure 2.6	(a) Schematic showing working of a heat pipe & (b) Basic Layout of Heat Pipe Based BTMS	40
Figure 2.7	Basic Schematic of PCM based BTMS	41
Figure 2.8	A schematic representation of a Hybrid BTMS	43
Figure 2.9	Graphical representation of comparison between different Battery thermal management system.	46
Figure 2.10	Classification of the factors influencing PCM-Based BTMS.	49
Figure 3.1	Measuring parameter values pulse current vs cell voltage response.	56
Figure 3.2	Typical Nyquist plot of a new li-ion battery cell	58
Figure 3.3	A general mth order Equivalent circuit model for a new li-ion battery cell	60

Figure 3.4	(a) Schematic of the setup, (b) Experimental Setup to obtain battery discharge parameters	62
Figure 3.5	Experimental data of the (a) open circuit voltage (OCV) and (b) discharge equivalent internal resistance of LiFePO <sub>4</sub> pouch cell	64
Figure 3.6	Curve fitted surface for (a) equivalent internal resistance, (b) open circuit voltage (OCV) and (c) entropy change $\left(\frac{dV_{OCV}}{dT}\right)$	66
Figure 3.7	Experimental setup illustrating the functional configuration for acquiring NMC Li-ion Battery discharge parameters and characteristics.	67
Figure 3.8	Variation of Experimental measurement of the (a) discharge internal resistance and (b) OCV of INR18650 cylindrical cell.	70
Figure 3.9	Electrochemical impedance spectra of the INR 18650 cylindrical Li-ion cell at (a) 100 % SoC, (b) 100 % SoC, (c) 50 % SoC, and (d) 25 % SoC	71
Figure 3.10	Two equivalent circuit model for li-ion battery— (a) with inductance and (b) without inductance.	74
Figure 4.1	Temperature profiles for 1 C – 4 C discharge rate of each model	93
Figure 4.2	Heat generation and Internal Resistance for each model at different (1 C – 4 C) discharge rate	94
Figure 4.3	Absolute relative errors for 1 C – 4 C discharge rate of each model	96
Figure 4.4	Voltage profiles for 1 C – 4 C discharge rate of each model	98
Figure 4.5	(a) Temperature and (b) Voltage profiles for 1 C – 4 C discharge rate of 2s2p Module	101
Figure 4.6	Temperature distribution of the LiFePO <sub>4</sub> pouch cell in a 2s2p module at various discharge rates captured at the end of discharge.	102
Figure 5.1	(a) Schematic of the Li-ion cell showing (i) 3D cross-sectional view of the cell components and (ii) 2D axisymmetric domain indicating boundary conditions, and (b) Three geometric configurations for analysing electrothermal behaviour	107
Figure 5.2	Equivalent circuit of $R_{int}$ model for Li-ion battery	110
Figure 5.3	Typical Nyquist plot for a Li-ion cell and its equivalent circuit model without an inductive element.	113
Figure 5.4	Typical Nyquist plot for a Li-ion cell and its equivalent circuit model with an inductive element.	115
Figure 5.5	Extracted ECM parameters for the circuit without inductance across different SoC and temperature conditions.	117
Figure 5.6	Extracted ECM parameters for the circuit with inductance across different SoC and temperature conditions.	118
Figure 5.7	Comparison of temperature evolution for three structural configurations against experimental data at (a) 1C and (b) 3C discharge rates, showing the impact of structural elements on thermal behaviour.	122
Figure 5.8	EIS fitting for the circuit without inductance at 50% SoC for 20 °C, 30 °C, 40 °C and 50 °C	124
Figure 5.9	EIS fitting for the circuit with inductance at 50% SoC for 20 °C, 30 °C, 40 °C and 50 °C	125

Figure 5.10	Comparison of temperature evolution profiles for the $R_{int}$ model, ECM without inductance, and ECM with inductance at (a) 1C and (b) 3C discharge rates.	127
Figure 5.11	Comparison of voltage evolution profiles for the $R_{int}$ model, ECM without inductance, and ECM with inductance at (a) 1C and (b) 3C discharge rates.	128
Figure 6.1	Sliding Window mechanism for data creation	135
Figure 6.2	Schematic of the (a) LSTM network architecture, (b) LSTM single layer, and (c) multi-layer neural network representation of the LSTM	138
Figure 6.3	Schematic of the Gate Recurrent Unit (GRU)	139
Figure 6.4	(a) Schematic of the Transformer Model (b) Multi-head Attention Mechanism (c) Multi-layer Encoder Decoder	143
Figure 6.5	Feature Correlation Heatmaps for Different Temperature Conditions (a) 4 °C, (b) 24 °C and (c) 43 °C	145
Figure 6.6	Actual vs. Predicted SoC Estimations using LSTM, GRU, and Transformer models at 4 °C, 24 °C, and 43 °C.	150
Figure 6.7	Comparison of RMSE for SoC Estimations across LSTM, GRU, and Transformer models at different temperatures.	151
Figure 6.8	RMSE variation with cycle number for SoC Estimation using LSTM, GRU, and Transformer models.	152
Figure 6.9	Comparison of RMSE for Voltage Estimations across LSTM, GRU, and Transformer models at different temperatures.	153
Figure 6.10	Actual vs. Predicted Voltage Estimations using LSTM, GRU, and Transformer models at 4 °C, 24 °C, and 43 °C.	154
Figure 6.11	RMSE variation with cycle number for Voltage Estimation using LSTM, GRU, and Transformer models.	155
Figure 6.12	Actual vs. Predicted Temperature Estimations using LSTM, GRU, and Transformer models at 4 °C, 24 °C, and 43 °C.	157
Figure 6.13	Comparison of RMSE for Temperature Estimations across LSTM, GRU, and Transformer models at different temperatures.	158
Figure 6.14	RMSE variation with cycle number for Temperature Estimation using LSTM, GRU, and Transformer models.	159
Figure 6.15	(a) Capacity vs. cycle number, (b) SoH vs Cycle number for different ambient temperatures (4°C, 24°C, and 43°C), (c) Evolution of $R_e$ and (d) $R_{ct}$ with cycle number	161
Figure 6.16	Correlation Heatmap of Electrothermal Parameters	162
Figure 7.1	Schematic of the Li-ion cell with a PCM based BTMS (a) 3D cross-sectional view of the Li-ion cell components with PCM BTMS, (b) 2D axial symmetric view showing boundary conditions.	168
Figure 7.2	DSC thermogram for (a) Latent heat, (b) Specific heat of the Capric acid, and (c) Differential scanning calorimeter (DSC) Q2000 from TA Instruments.	171
Figure 7.3	(a) Grid and (b) Time step independence study for variation of average surface temperature with time.	178

Figure 7.4	Schematics of the structured mesh for the Li-ion cell with PCM based BTMS	178
Figure 7.5	Comparison of (a) Melt fraction variation Kamkari et al.[9] for PCM model validation and (b) Cell surface temperature at different discharge rates for Battery thermal model validation.	180
Figure 7.6	Instantaneous Variation of Melt Fraction and Temperature contours at different times against experimental results [9].	180
Figure 7.7	Average cell surface temperature at different discharge C rates.	181
Figure 7.8	Distinct stages or intervals cell surface temperature variation of the 18650 cylindrical Li-ion without utilizing PCM at (a) 1.0 C and (b) 3.5 C discharge rate.	181
Figure 7.9	Comparison of (a) heat generation and (b) internal resistance inside the INR 18650 cylindrical Li-ion cell at different discharge rates.	182
Figure 7.10	Effect of PCM thickness on Battery surface temperature during (a) 1 C discharge rate, (b) 3.5 C discharge rate.	183
Figure 7.11	(a)Temperature and (b)Melt fraction contours at 3.5 C discharge rate considering the effect of PCM thickness.	184
Figure 7.12	(a) Melt Fraction and (b) Energy stored within the phase change material (PCM) at different discharge rates for different PCM thickness.	185
Figure 7.13	Variation of Battery surface temperature evolution and Melt fraction for (a) 2.5 C, (b) 3.0 C and (c) 3.5 C discharge rate.	186
Figure 7.14	(a) Maximum and (b) Minimum surface temperatures of 18650 Li-ion cell at different discharge rate.	186
Figure 7.15	Comparison of $T_i^*$ and $\Delta T_i^*$ at different discharge rate.	187
Figure 7.16	Comparison of (a) Cell Cooling Coefficient (CCC) and (b) PCM cooling enhancement factor for different PCM thickness configurations at varying discharge current ratings.	190
Figure 7.17	(a) Gravimetric and (b) Volumetric energy densities of Li-ion cells after integrating PCM based thermal management system.	192
Figure 8.1	Decision hierarchy of PCM selection.	197
Figure 8.2	Flowchart of the general procedure for AHP weight assignment.	199
Figure 8.3	Relative attribute weights for PCM selection using Analytical Hierarchy Process (AHP)	200
Figure 8.4	Battery temperature reduction using top five PCMs selected based on global TOPSIS ranking.	209
Figure 8.5	Battery temperature reduction using top-performing PCMs selected from temperature-window-based TOPSIS segmentation.	211
Figure 8.6	Model configuration for passive cooling: (a) 3D view of a Li-ion cell with PCM or immersion coolant, (b) 2D axisymmetric domain with applied boundary conditions	213
Figure 8.7	Variation of Battery surface temperature evolution	218
Figure 8.8	Comparison of Energy Density (Wh/kg)	220

Figure 8.9	Thermal performance of a cylindrical battery module under 3.5 C discharge rate: (a) Temperature distribution across the module at the end of discharge; (b) Time evolution of the average pack temperature	222
Figure 9.1	Model configuration for the hybrid battery thermal management system (BTMS), showing coolant flow representation and the computational domain.	226
Figure 9.2	Temperature evolution of the battery pack at (a) 3C and (b) 3.5C discharge rates, comparing PCM-only cooling with the hybrid BTMS.	232
Figure 9.3	Indian Driving Cycle (IDC) velocity profile used as a power demand input for evaluating the integrated battery and cabin thermal management system.	234
Figure 9.4	Simulink model architecture of the integrated battery and cabin thermal management system.	235
Figure 9.5	Transient temperature response of the cabin and battery pack at 25 °C ambient temperature.	237



## List of Tables

Table Number	Description	Page No.
Table 1.1	Characteristics of different chemistry of Li-ion batteries [5]	8
Table 2.1	Comparison of different Battery thermal management system	47
Table 4.1	LiFePO <sub>4</sub> -20Ah pouch cell technical specifications	78
Table 4.2	Correlation for estimating the thermophysical properties of Li-ion cell	82
Table 6.1	RMSE for SoC Estimations across LSTM, GRU, and Transformer	150
Table 6.2	RMSE for Voltage Estimations across LSTM, GRU, and Transformer	153
Table 6.3	RMSE for Temperature Estimations across LSTM, GRU, and Transformer	158
Table 7.1	Thermophysical properties of different layer of INR (Lithium Nickel Manganese Cobalt Oxide (NMC)) 18650 cylindrical cell [10–12].	169
Table 7.2	Thermal properties of the Active zone of Li-ion battery and outer casing.	170
Table 7.3	Thermal properties of Capric acid [13–17].	170
Table 8.1	Results obtained from AHP method	200
Table 8.2	Material selection attributes values according to a decisive 11-point scale. [15,170]	202
Table 8.3	Decision matrix of selected Phase Change Materials (PCMs) based on ten evaluation attributes	205
Table 8.4	Ranking of the top ten Phase Change Materials (PCMs) based on the TOPSIS method	206
Table 8.5	Thermophysical properties of different coolants [18]	217
Table 9.1	Thermophysical properties of PCM and coolant	227
Table A.1	Experimental value of OCV (V) at various depth of discharge (DoD) and Temperature ranges.	271
Table A.2	Experimental value of discharge equivalent internal resistance ( $\Omega$ ) at various depth of discharge (DoD) and Temperature ranges.	272
Table A.3	Summary of uncertainty analysis.	273
Table C.1	Specifications of the INR 18650 Lithium-ion cell in terms of technical details.	279
Table C.2	Experimental measurement of Open Circuit Voltage (V) across different temperature range and SoC levels.	279
Table C.3	Experimental measurement of discharge internal resistance across different temperature range and SoC levels.	280



## List of Symbols

Symbol	Description
$g$	Acceleration due to gravity, (m/s <sup>2</sup> )
$d_{cell}$	Diameter of cell, (mm)
$\rho$	Density
$I_{cell}$	Discharge Current, (Ampere)
$R_{int}$	Discharge Internal Resistance, ( $\Omega$ )
$q_{reversible}$	Entropic heating, (W)
$Q_h$	Heat generation, (W/m <sup>3</sup> )
$h_{cell}$	Height of cell, (mm)
$\theta$	Melt Fraction
$k$	Thermal conductivity, (W/m °C)
$t$	Time, (s)
$u$	Velocity vector, (m/s)
$V_{batt}$	Volume of cell, (m <sup>3</sup> )
$C_{mush}$	Mushy zone constant
$V_{ocv}$	Open Circuit Voltage, (V)
$c_p$	Specific heat capacity, (J/kg °C)
$T$	Temperature, (K)
$k$	Thermal conductivity, (W/m °C)

## List of Abbreviations

Abbreviation	Abbreviation
BMS	Battery management system
BTMS	Battery thermal management system
CCC	Cell cooling coefficient
cPCM	Conductive composite phase change material
CC	Constant Current
DoD	Depth of discharge
EVs	Electric vehicles
EIS	Electrochemical Impedance Spectroscopy
ESS	Energy storage system
GHG	Greenhouse Gas
HEVs	Hybrid Electric Vehicles
ICE	Internal Combustion Engine
LFP	Lithium iron phosphate
LiB	Lithium-ion Battery
LMO	Lithium-ion manganese oxide
NMC	Nickel Manganese Cobalt Oxide
PCM	Phase change material
SEI	Solid Electrolyte Interphase
SoC	State of charge